LABORATORI NAZIONALI DI FRASCATI
SIS – Pubblicazioni

LNF–95/007 (P)
20 Febbraio 1995

Two Photon Interaction Measurements with the KLOE Small Angle Tagging System

F. Anulli[1], R. Baldini Ferroli[1], M. Bassetti[1], A. Courau[2], I. Cohen[3], A. Moalem[4], G. Pancheri[1], M. Preger[1], L. Razdolskaja[4], P. Sergio[1], A. Zallo[1]

1) INFN – Laboratori Nazionali di Frascati, P.O. Box 13, I 00044–Frascati (Roma) Italy
2) Laboratoire de l'Accelerateur Lineaire, CNRS–IN2P3, Universite de Paris–Sud, 91405 Orsay, France
3) School of Physics and Astronomy, Tel–Aviv University Raimond and Beverly Sackler Faculty of Exact Sciences – 69978 Tel Aviv, Israel
4) Department of Physics, Ben–Gurion University, 84105 Beer–Sheva, Israel

Abstract

The two-photon processes $\gamma\gamma \to \pi^0, \eta, \pi^0\pi^0, \pi^+\pi^-, \pi^0\eta, \eta'$, expected in e^-e^+ collisions at DAΦNE, can be studied with high precision by introducing a small angle tagging facilities for the scattered electrons. We describe the design of the KLOE small angle tagging system to study $\gamma\gamma$ interactions at DAΦNE. This includes a COIL detector to tag particles hitting the SFM coils, a SAT detector to tag electrons passing through the SFM and a BREM detector for high energy photons in coincidence with tagged electrons in order to reject the radiative Bhabha events. Two such systems placed symmetrically with respect to the interaction point allow tagging both electrons and positrons. The maximum number of events/year that can be collected by this tagging system and the statistical error on the $\gamma\gamma \to \pi^0\pi^0$ cross section are also discussed.

PACS.: 13.60.Le; 29.90.+r

Contribution to the "Second DAΦNE Physics Handbook"

1 Introduction

We address here the question of the feasibility of photon-photon scattering in electron positron collisions at DAΦNE. We shall estimate event rates with $L = 5 \times 10^{32} cm^{-2} s^{-1}$ for a nominal year of running time $\Delta t = 10^7\ s$. With such high luminosity and the high resolution expected by the KLOE detector, we believe that there is a realistic chance to gather a large number of events for these processes, even though one would expect the portion of phase space accessible for $\gamma\gamma$ physics at a 1 GeV c.m. e^+e^- machine like DAΦNE to be rather small. That being certainly the case, the combination of high luminosity and full angular coverage should allow for a more extended use of the available phase space than other higher energy, but so far lower luminosity, machines. To illustrate these two points in a quantitative fashion, consider the general expression for processes of the type

$$e^+e^- \rightarrow e^+e^- + \gamma\gamma \rightarrow e^+e^- + X\ , \tag{1}$$

with c.m. energy $\sqrt{s} = 2E$. With x_1 and x_2 the fractional electron energy carried by the photons, the available phase space is proportional to the area element $\mathcal{A} = d(lnx_1)d(lnx_2)$. It was noticed [1] that the constraints on the available phase space compare very favorably with the detector acceptance and that the KLOE detector, unlike what happens to detectors in higher energy machines, should be able to collect all the interesting events in two photon physics. In other words, while it is true that phase space is limited, one can make full use of it. A similar point can be made concerning the gamma gamma luminosity. In the Double Equivalent Photon Approximation, the cross-section, for a given energy of the two photon system in their c.m. frame, can be written as

$$\frac{d\sigma}{dW_{\gamma\gamma}} = \frac{dL}{dW_{\gamma\gamma}} \hat{\sigma}(\gamma\gamma \rightarrow X)\ , \tag{2}$$

with the two photon distribution given by

$$\frac{dL}{dW_{\gamma\gamma}} = \frac{4}{W_{\gamma\gamma}} (\frac{\alpha}{\pi} \ln \frac{E}{m_e})^2 [(2+z^2)^2 \ln \frac{1}{z} - (1-z^2)(3+z^2)]\ ; \quad z = \frac{W_{\gamma\gamma}}{2E}\ . \tag{3}$$

Using this two photon flux and the machine luminosity, one can calculate the gamma gamma differential luminosity shown in Fig. 1 for two possible values of the energy at which DAΦNE will operate, $\sqrt{s} = m_\phi = 1.020\ GeV$ and the maximum project energy $\sqrt{s} = 1.5\ GeV$.
To make the appropriate comparison, the fluxes, for a nominal 100 days of running time, have been evaluated at the DAΦNE project luminosity mentioned in the introduction and at present LEP luminosity, $L = 10^{31}\ cm^{-2}\ sec^{-1}$ [2]. From the figure, we see that in the region $W_{\gamma\gamma} \leq 600\ MeV$, the two photon flux expected at DAΦNE is as large, and even larger, than at LEP. Such a comparison fails completely beyond the threshold region for hadronic processes, but it shows the advantage of high luminosity for studying one and two pion production.

In what follows, we shall first estimate the number of events expected in some channels of interest and their possible backgrounds and the need for electron tagging to eliminate physical background. Secondly we shall describe the proposed tagging system.

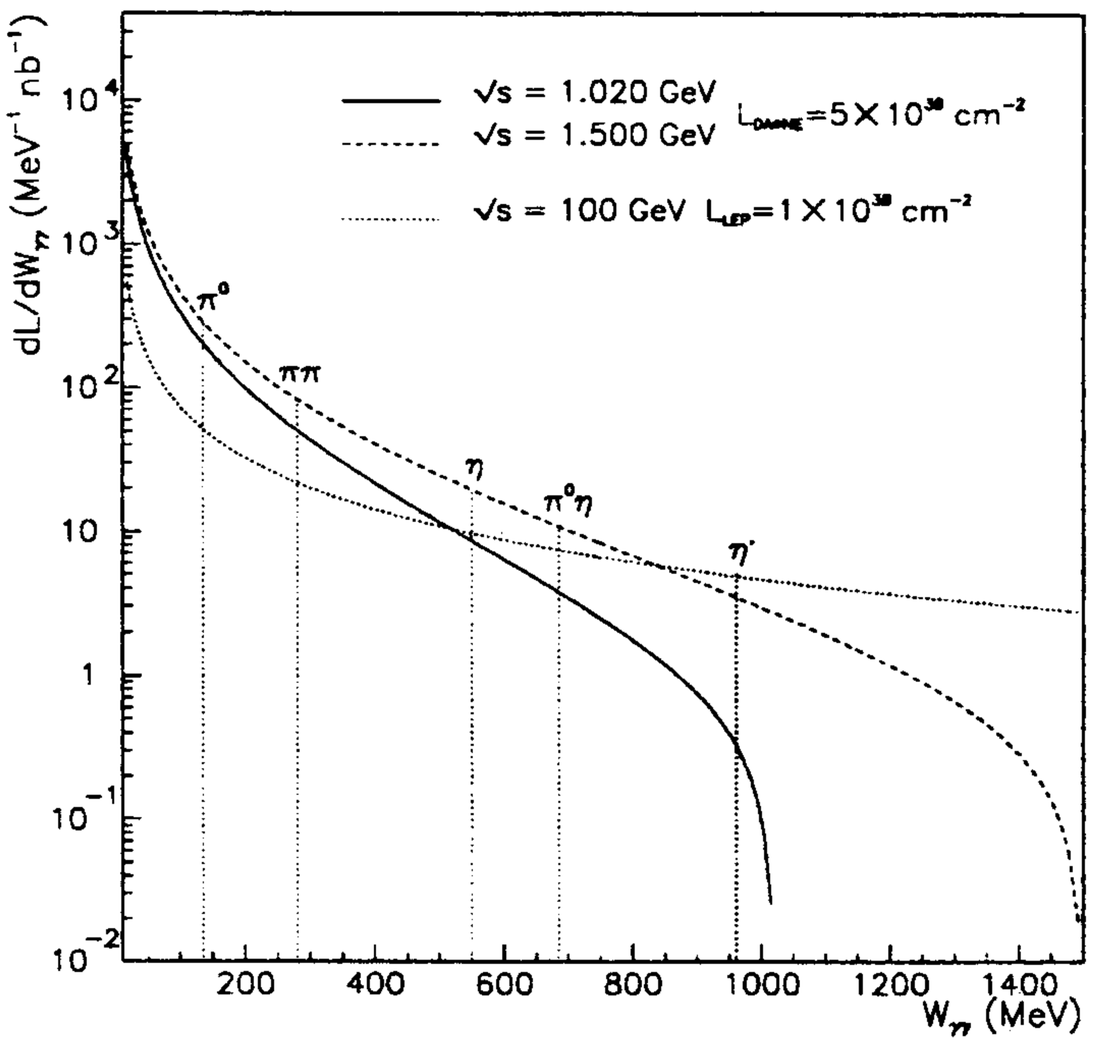

Figure 1: Photon-photon luminosity at DAΦNE, for an integrated machine luminosity $L = 5\ fb^{-1}$ per year, and at LEP with the present integrated luminosity $L_{LEP} = 0.1\ fb^{-1}$ per year. Thresholds for various physical processes of interest at DAΦNE are shown.

2 Cross-sections for hadron production

The hadronic final state processes of interest at DAΦNE are limited to

$$\gamma\gamma \rightarrow \pi^0, \eta, \pi^0\pi^0, \pi^+\pi^-, \pi^0\eta, \eta' \quad .$$

The observation of the last two processes being possible only at the higher DAΦNE energy, $\sqrt{s} = 1500\ MeV$. In the DEPA, the cross section for production of a pseudoscalar meson of mass M_P can be written in the narrow width approximation as [3],

$$\sigma(ee \rightarrow ee + P) = \frac{64\alpha^2}{M_P^3} \ln^2\left(\frac{E}{m_e}\right) \ln\left(\frac{2E}{M_P}\right) \Gamma(P \rightarrow \gamma\gamma) \ ,$$

where $\Gamma(P \rightarrow \gamma\gamma)$ is the radiative width for which one writes,

$$\Gamma(P \rightarrow \gamma\gamma) = \frac{\alpha^2}{32\pi^3} \frac{M_P^3}{f_P^2} \left[\sum_{colors} < e_q^2 >\right]^2 \quad . \tag{4}$$

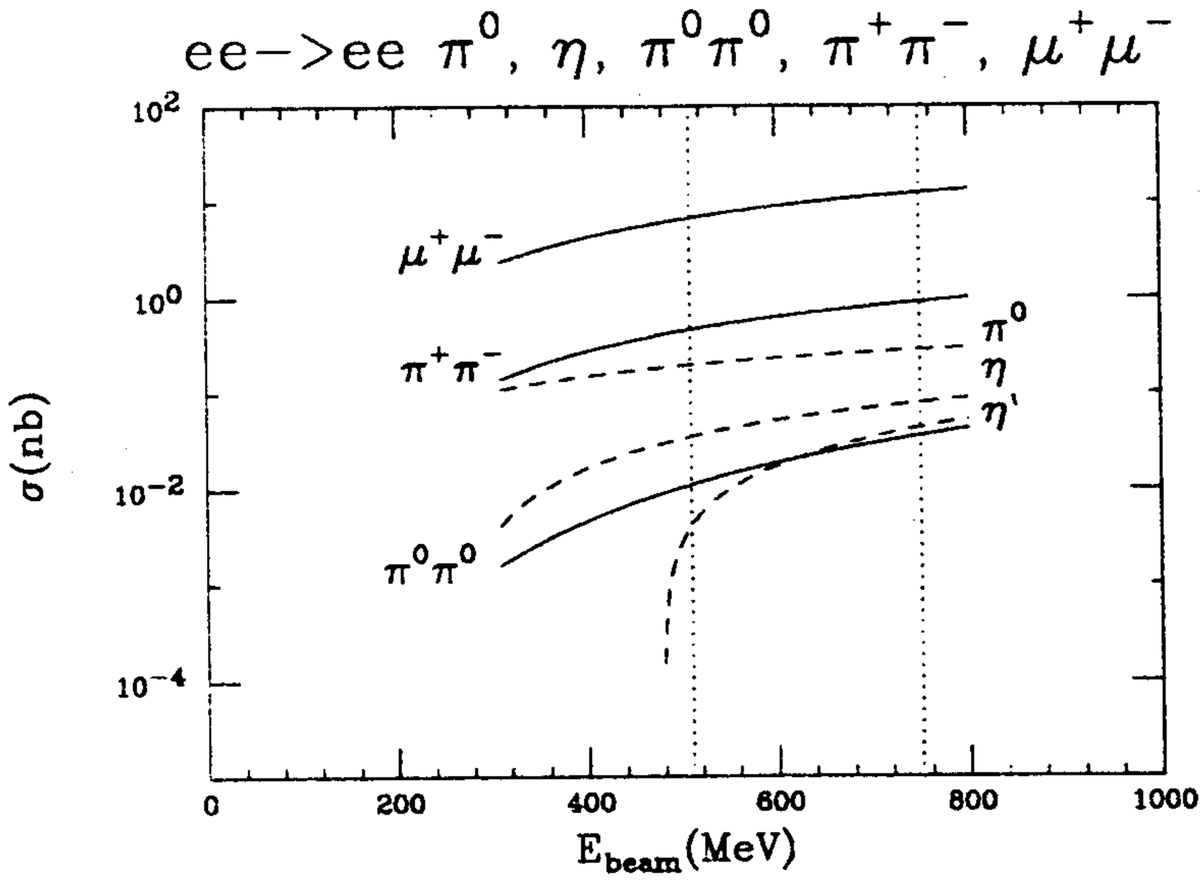

Figure 2: Examples of two photon cross-sections in the DAΦNE energy region, in the DEPA, as a function of the beam energy.

In eq.(4), e_q is the quark charge which couples to the photon and f_P is the decay constant. For the cases of π^0, η and η', the three radiative widths are expressed in terms of three parameters, the mixing angle (θ) and the decay constant of the pseudoscalar singlet (f_1) and octet (f_8). Combining these different widths, it is possible to obtain a relation from which one can extract information on the mixing angle by measuring η and π^0 radiative widths, i.e.

$$\frac{\Gamma(\eta \to \gamma\gamma)}{\Gamma(\pi^0 \to \gamma\gamma)} = \frac{1}{3}\left(cos\theta - 2\sqrt{2}sin\theta\right)^2 \left(\frac{m_\eta}{m_\pi}\right)^3 .$$

Subsequently, when DAΦNE will operate at higher energy, one will be able to use a second relation between these quantities, which is independent of the mixing angle, and which can test the SU(3) limit $f_1 = f_8$, i.e.

$$R = \left[\frac{\Gamma_\eta}{m_\eta^3} + \frac{\Gamma'_\eta}{m_{\eta'}^3}\right]\frac{m_\pi^3}{\Gamma_\pi} = \frac{1+8r^2}{3} \; ; \quad r = \frac{f_1}{f_8} .$$

R=3 corresponds to r=1. Present measurements[2] give,

$$R = 2.5 \pm 0.5(stat) \pm 0.5(syst) .$$

Using the one loop chiral perturbation theory calculations [4, 5] for the charged pion process and a phenomenological fit to the Crystal Ball data [6] for two π^0 production, close to the

Table 1: $(e^-e^+ \to e^-e^+PS)$ events/year

Meson[1]	Total Production Rate	E_{beam}
π^0	2.0×10^6	$510\ MeV$
η	5.0×10^5	$510\ MeV$
η'	1.0×10^5	$750\ MeV$

dispersive analysis of ref [7], one obtains the production cross-sections displayed in Fig. 2. Providing one can overcome the strong QED background which affects these processes, measurements at DAΦNE are expected to be of considerable improved statistical accuracy. To estimate the expected number of events for these processes, we integrate eq.(2) over the two photon c.m. energy $W_{\gamma\gamma}$. For pseudoscalar meson production, the yearly yield is shown in Table 1. For the two body processes, integrating the differential number of events shown in Fig. 3 over the two photon energy, we get a total yield of $\simeq 10^4$ for $\pi^0\pi^0$ and $\simeq 10^6$ for $\pi^+\pi^-$. These estimates are rather encouraging, as they indicate a large event statistics. By far, the most dangerous source of background for the processes discussed before comes from,

$$\phi \to K_S K_L \to \pi^0\pi^0 + X(undetected)\ , \tag{5}$$

where the K_L escapes detection with a 25% probability [8]. This cross-section is rather large, since,

$$\sigma(e^+e^- \to \pi^0\pi^0 + X) = \sigma_\phi \times BR(\phi \to K_L K_S) \times BR(K_S \to \pi^0\pi^0) \times P(K_L\ escape)\ .$$

With $\sigma_\phi = 4.4\ \mu b$ and $P(K_L\ escape) = 0.25$, we see that process (5) completely overcomes the signal of interest. Other potential background processes are indicated in Table 2, along with the expected number of events they contribute to the $\gamma\gamma$ rate of interest. In order to identify the signal, one can plot mass and transverse momentum distribution for both the genuine $\gamma\gamma \to \pi^0\pi^0$ as well as for the background processes. For the particular case of process (5), Fig. 4 shows that background and signal have very different event distributions, and one may devise appropriate kinematical cuts to isolate the signal, e.g. a transverse momentum cut on the two π^o system at $p_t^2 \geq 2000\ MeV^2/c^4$.

Such cut will indeed reduce by a factor 25 the total background from process (5), but the enormous difference in scale between the shaded and non-shaded area in Fig. 4 may prevent in practice the isolation of the genuine $\gamma\gamma$ events. It is therefore clear that this measurement will only be possible by introducing a small angle tagging system for the electrons, as described in the next section. We note though that even with tagging, this measurement is far from being background free. Indeed, the tagged electrons emerge at very small angles, an angular range where electron rates from radiative Bhabha ($e^+e^- \to e^+e^-\gamma$) and double radiative Bhabha ($e^+e^- \to e^+e^-\gamma\gamma$) scattering as well as from beam-gas bremsstrahlung is expected to be very high. A simple and compact expression for the radiative Bhabha cross-section rate in the small angle region, recently obtained in a no-recoil approximation

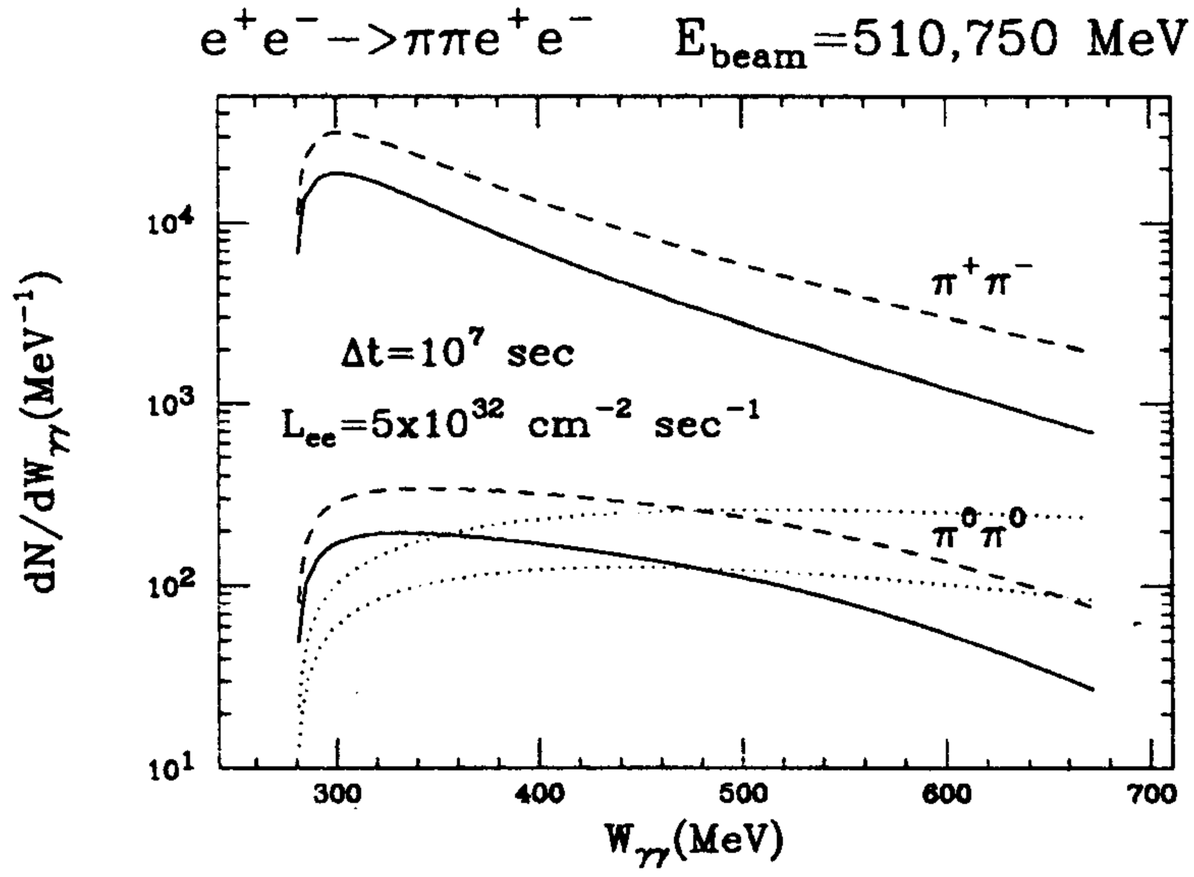

Figure 3: Number of events per MeV vs. two photon c.m. energy. Solid and dashed lines correspond to the DAΦNE energies, $E_{beam} = 0.51$ and 0.75 GeV respectively. For $\pi^0\pi^0$, the results are obtained using a phenomenological fit to the Crystal Ball data and the dotted lines correspond to the 1-loop chiral perturbation theory calculation.

Table 2: Background from Annihilation Events

ϕ Decay Mode[1]	Escaped Particle[3]	Events/Year[2]	$\gamma\gamma$ Process
$K_S^0(\pi^0\pi^0)\ K_L^0$	K_L^0	5.3×10^8	$\pi^0\pi^0$
$\eta(3\pi^0)\ \gamma$	π^0, γ	8.4×10^5	$\pi^0\pi^0$
$K_S^0(\pi^+\pi^-)\ K_L^0$	K_L^0	1.1×10^9	$\pi^+\pi^-$
$\rho(\pi^+\pi^-)\ \pi^0$	π^0	2.6×10^7	$\pi^+\pi^-$
$(\pi^+\pi^-)\ \pi^0$	π^0	4.8×10^6	$\pi^+\pi^-$
$\eta(\pi^+\pi^-\pi^0)\ \gamma$	π^0, γ	6.2×10^5	$\pi^+\pi^-$

1) The particles in parentheses are assumed to be detected in KLOE.
2) Events/year corresponds to 2×10^{10} $\phi(1020)$ produced per year.
3) The escape probability of the γ is not included.

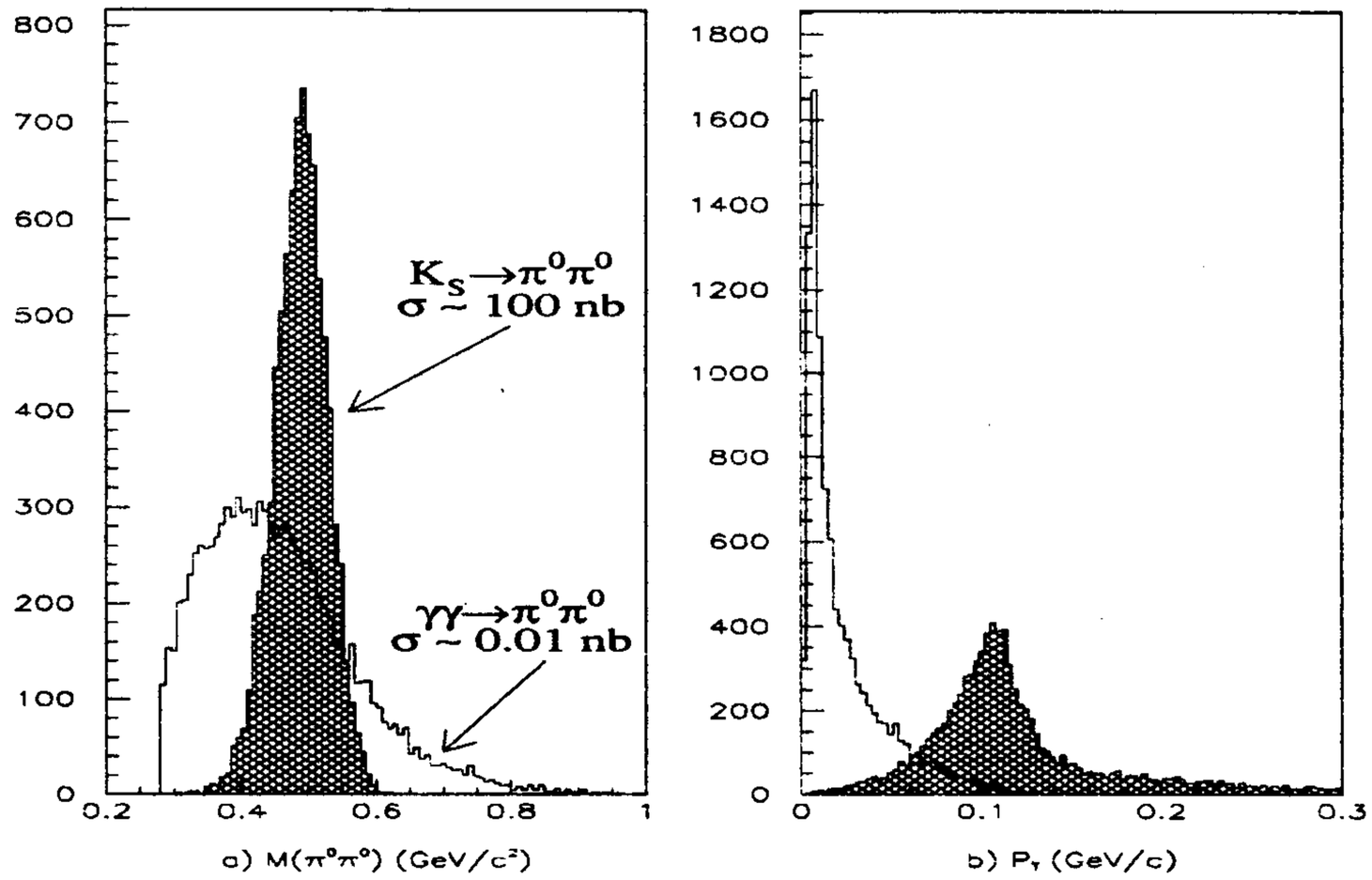

Figure 4: a) invariant mass distribution of $\pi^0\pi^0$ system from $\gamma\gamma$ events or K_S decays. b) Transverse momentum distribution of $\pi^0\pi^0$ system. The two histograms are not normalized and should be scaled according to the relative cross-sections. The integrated area of the $\gamma\gamma \to \pi^0\pi^0$ peak is roughly 10^{-4} that of the $K_S \to \pi^0\pi^0$.

[9], reads,

$$\frac{d\sigma}{dkdt} = \frac{4\pi\alpha^2}{t^2}\frac{\beta(t)}{k}\frac{E^2+(E-k)^2}{2E^2} \quad ,$$

where k is the energy of the radiated photon, t is the square of the electron transferred momentum, and the photon spectrum $\beta(t)$ is calculated to be,

$$\beta(t) = \frac{4\alpha}{\pi}\left[\frac{2m_e^2-t}{\sqrt{-t}\sqrt{4m_e^2-t}}log\frac{\sqrt{4m_e^2-t}+\sqrt{-t}}{\sqrt{4m_e^2-t}-\sqrt{-t}} - 1\right] \quad .$$

The single gamma radiative Bhabha cross section, integrated over all the SAT acceptance has been evaluated to be $\simeq$ 70 *mbarn* at most [9, 10]. As discussed later, this is an acceptable rate, which should allow implementation of single and double tagging in the very forward region, in coincidence with measurement of two pions in the KLOE detector.

3 The small angle tagging system

In ref [8] it has been shown that high precision measurements of two-photon reactions can be performed by equipping KLOE with tagging facilities both at wide and small angle. The

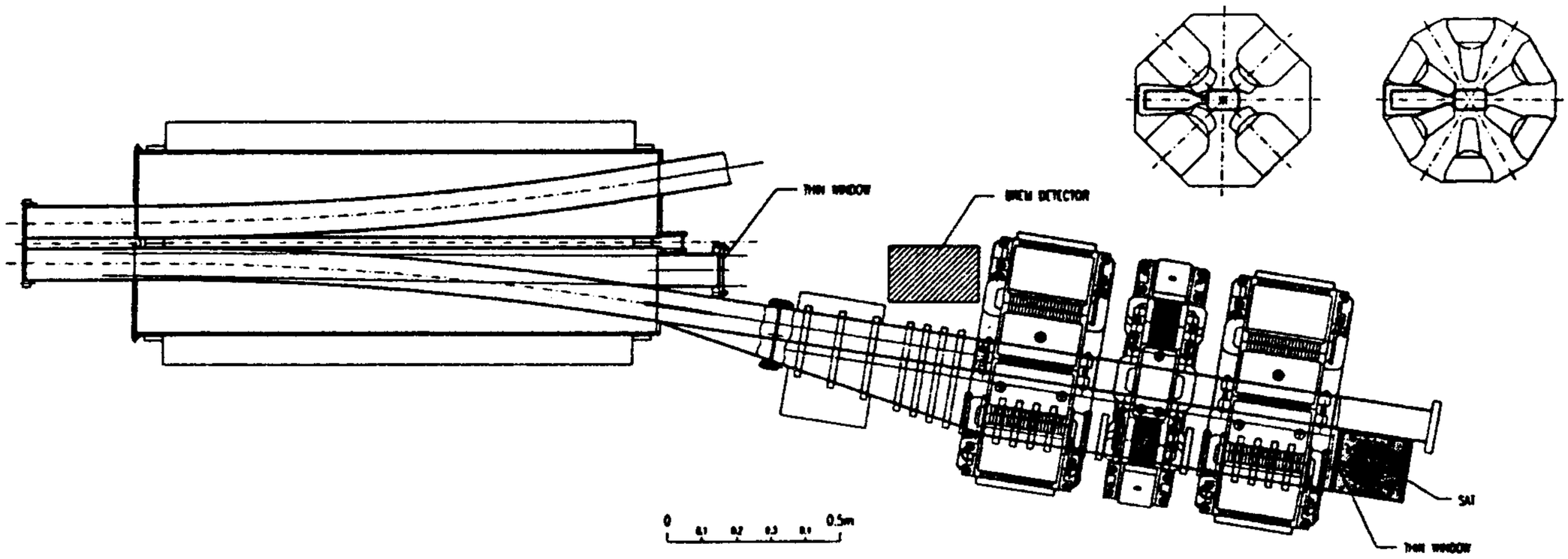

Figure 5: The new DAΦNE layout near the SAT area. The main modifications with respect to the standard structure are the two large quadrupoles, the sextupole and the large vacuum chamber. Cross section of these elements are shown to the right on top.

small angle tagging system, for electrons scattered at less than 20 *mrad*, will be located downstream of the interaction region, after the first bending magnet (Split Field Magnet), see Fig. 5, while the wide angle tagging will be incorporated in the KLOE detector. In the following we will discuss only the small angle tagging system.
This system includes a COIL detector to tag electrons hitting the Split Field Magnet (SFM) coils, a SAT detector to tag electrons passing through the SFM and a BREM detector for the rejection of radiative Bhabha events. Two such systems placed symmetrically with respect to the interaction point allow tagging both electrons and positrons.
The angular and energy distributions of electrons reaching the SFM region together with the corresponding $\gamma\gamma$ invariant mass are shown in Fig. 6. As it can be seen from the horizontal and vertical profile distributions displayed in Fig. 7, the $\gamma\gamma$ electrons are spread all over the SFM entrance face. The largest part of these ($\simeq$ 27% of the total production rate) enters the SFM and can be used for tagging. There is a sizable fraction ($\simeq$ 11.5%) of electrons with horizontal dispersion $x < 1.5\ cm$ with respect to the SFM axis and thus hit the coils. These can also be detected by placing a small detector in front of the coils as will be described in the following. Few electrons enter the vacuum chamber of the other beam ($\simeq$ 3%) and are lost. Due to vacuum requirements the tagging systems must be placed outside the beam pipe and collect only those particles which are separated from

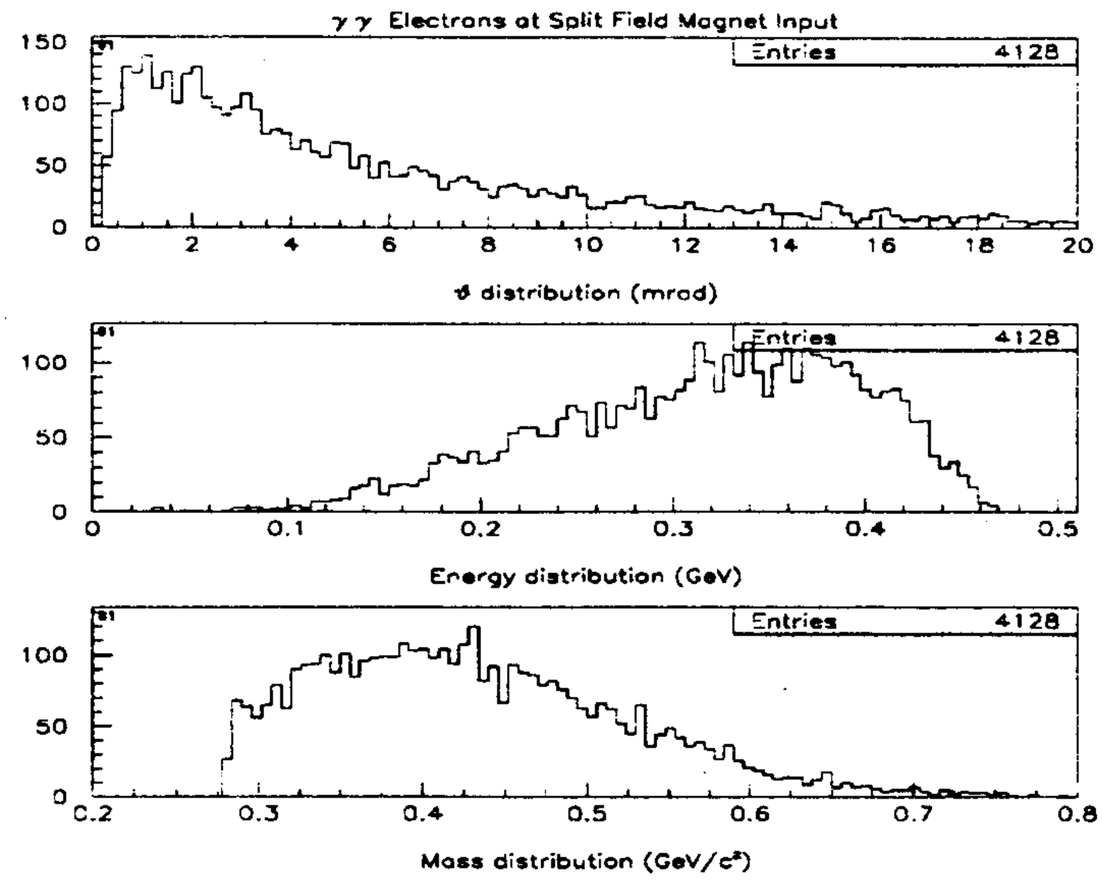

Figure 6: Angular and energy distributions of the scattered electron at the Split Field Magnet input. The invariant mass of the corresponding hadronic systems produced is shown at the bottom.

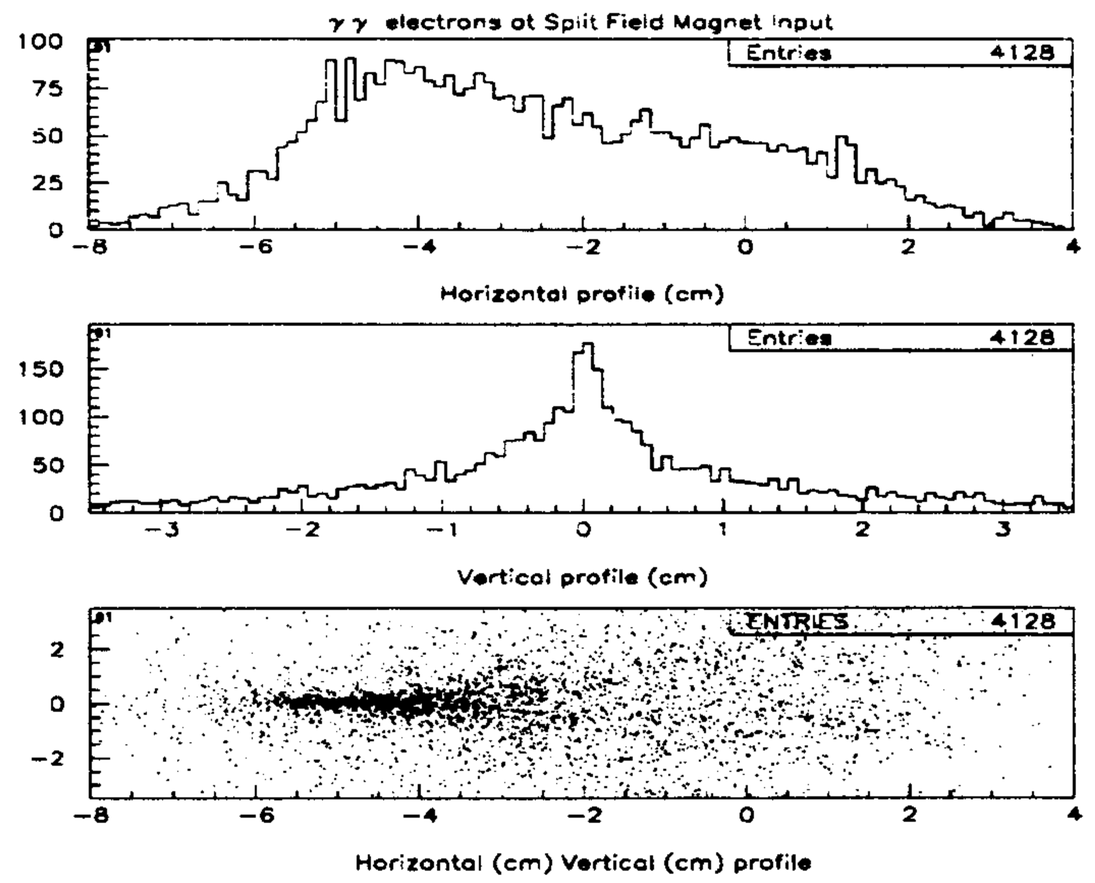

Figure 7: Horizontal and vertical profile distributions of electrons reaching the Split Field Magnet input. Coordinates are measured with respect to the machine symmetry axis.

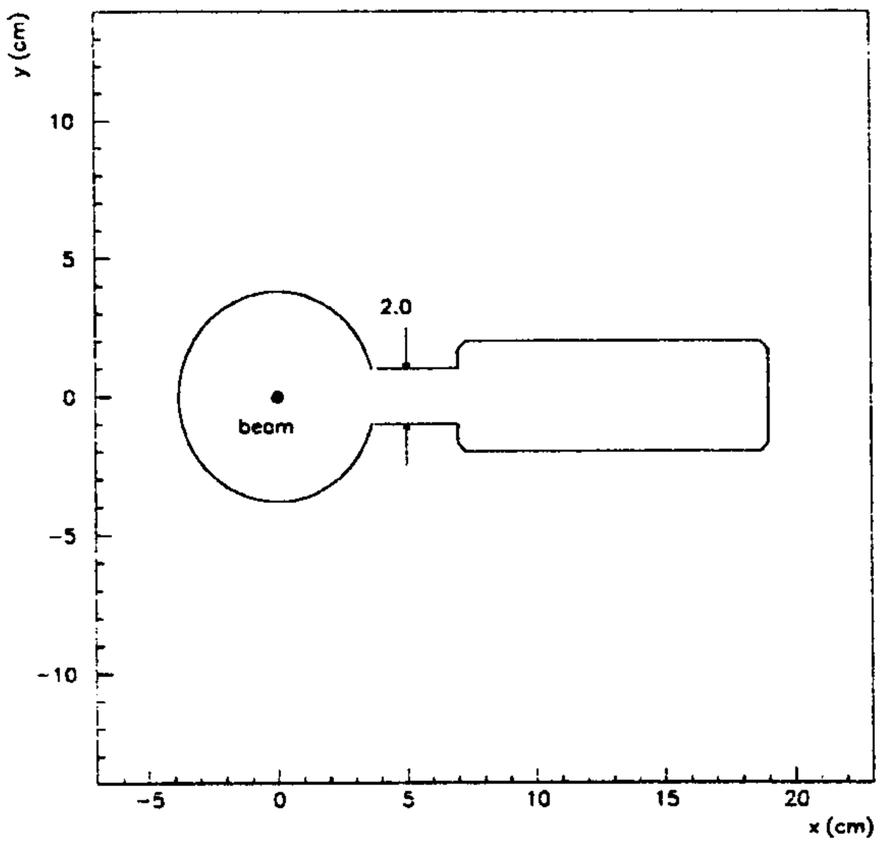

Figure 8: A sketch of the beam pipe section at the SAT position.

the primary beam by more than $\simeq 5$ *cm*. The machine elements which follow the SFM include a focusing quadrupole, a sextupole and a second defocusing quadrupole [11]. We have decided to locate the small angle tagging system (SAT) at a distance of $\simeq 8.65$ *m* from the interaction point, just after the second defocusing quadrupole, covering a horizontal separation of -5 to -30 *cm* with respect to the primary beam. This requires that the three elements following the SFM must have sufficiently large horizontal aperture. We assume the quadrupoles and sextupole have $\simeq \pm 1.5$ *cm* vertical and $\simeq \pm 30.0$ *cm* horizontal apertures. Elements of these kind are already foreseen in the main rings. The electrons cross the vacuum chamber walls at small angles (x' ranges from 40 to 100 *mrad*). In order to avoid Coulomb scattering and γ conversion effects the amount of material seen by the electrons needs to be minimized. Enlarging the beam pipe near the tagging site would increase the overall broadband impedance of the ring. Therefore, we adopt the solution shown in Fig. 8, proposed to us by the machine group. The standard cylindrical beam pipe is connected to an external chamber through a vertical aperture of $\simeq \pm 1$ *cm* extending from the SFM exit to the defocusing quadrupole. In order to account for the electron dispersion, the horizontal extension of the vacuum chamber increases along the beam line. The thickness of the thin window in front of the SAT should not be more than 100 μ steel.

3.1 The SAT detector

The fraction of ring layout relevant to the tagging system is shown in Fig. 5. Sketched in this figure is the SAT system to be located just after the second defocusing quadrupole. Because of the particular shape of the vacuum chamber and the characteristics of the large magnets required in this area, the SAT acceptance for single tagging is reduced from $\simeq 27\%$

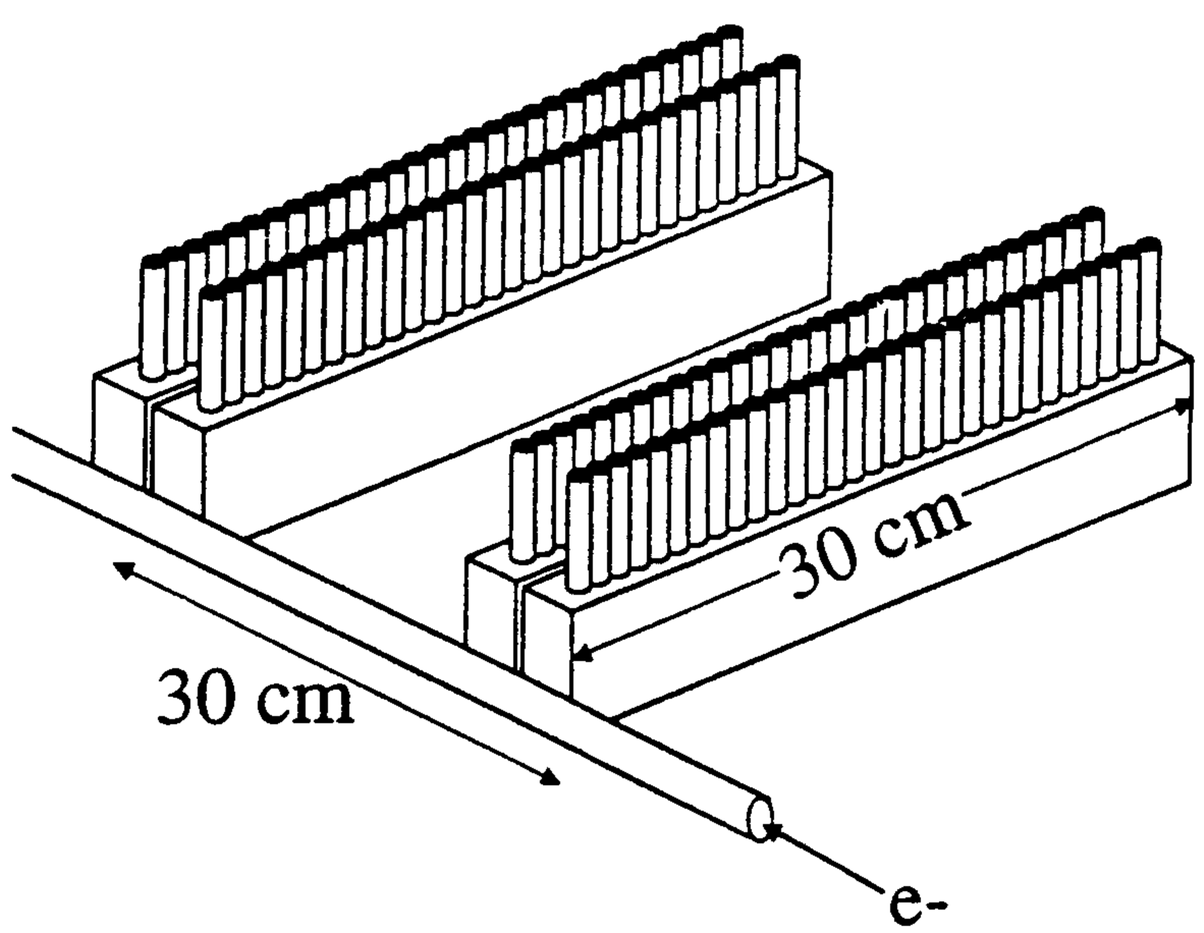

Figure 9: A sketch of the small angle tagger SAT. It is built as two hodoscopes at a distance of 30.0 *cm*. Each hodoscope is composed of two parallel planes of scintillating fibers of 1.0 *cm* diameter bundles, staggered with respect to each other by 0.5 *cm*.

to $\simeq 14\%$ only. An identical detection system is located on the other side of the interaction region to tag the positrons so that the single tagging acceptance is doubled. Let us consider now the design of the SAT detector, tailored to the properties of the electrons to be tagged and the expected background. Its main functions are:
1) record the electrons from $\gamma\gamma$ events,
2) determine the hit position in the horizontal direction (x coordinate) which in turn determines the electron energy,
3) identify the hitting particle, *i.e.*, separate electrons from muons and pions,
4) eliminate other background sources such as electrons from radiative Bhabha scattering.
As will be described in subsection 3, the rate of radiative Bhabha at the SAT position is rather high so that the SAT must be a fast detector. Many of the functions mentioned above can be achieved with the structure displayed in Fig. 9. The detector is composed of two 30.0 *cm* wide $\times$ 7.0 *cm* high hodoscopes, placed 30 *cm* apart along the beam direction. Each hodoscope is composed of two parallel planes of scintillating fibers of 1.0 *cm* diameter bundles, staggered with respect to each other by 0.5 *cm*. There is a photomultiplier juxtaposed on top of each bundle set in the vertical plane. The fibers (1 *mm* in diameter) run parallel to the bundle axis and their total length is estimated to be $\approx$ 1 *km* for each SAT detector. Two such hodoscopes provide position (x) and

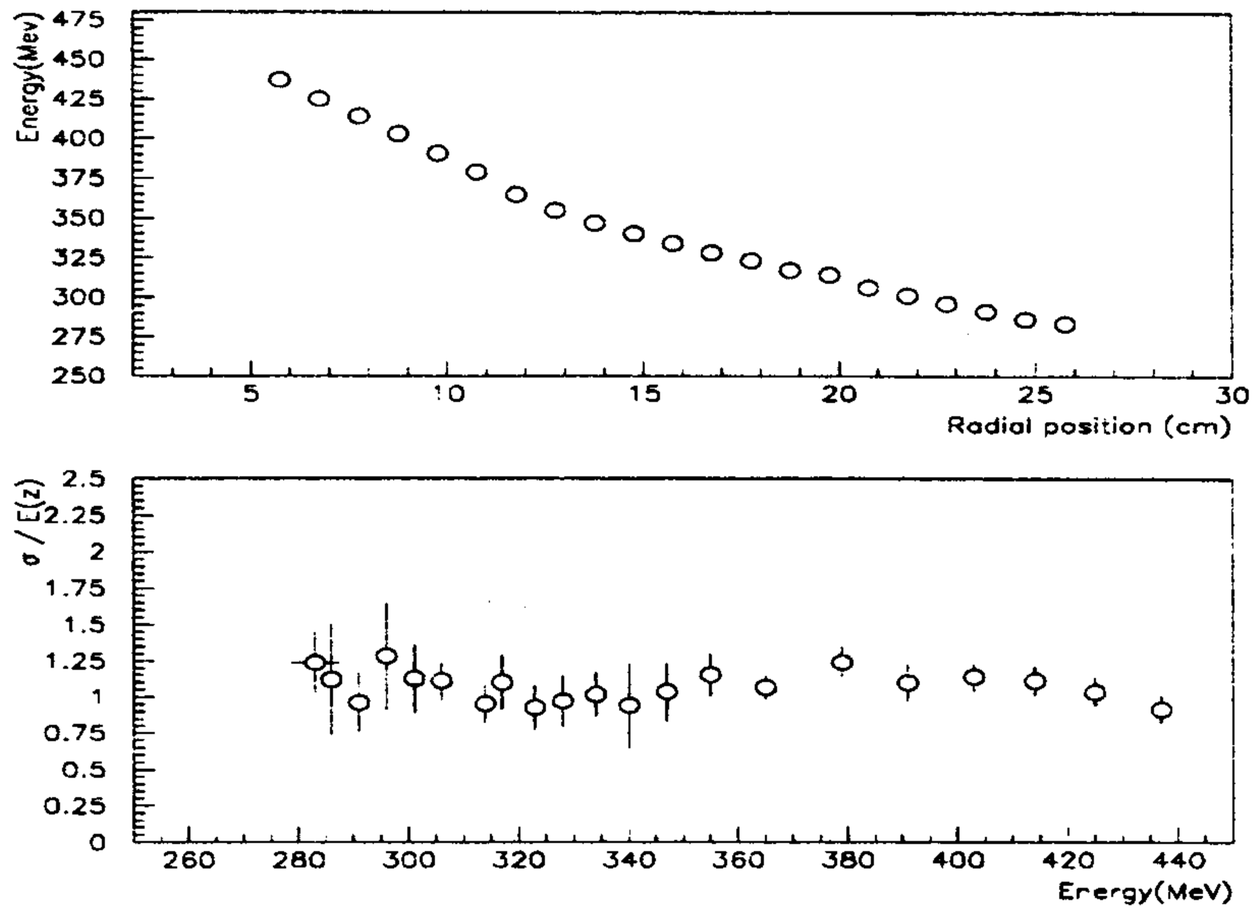

Figure 10: Energy-position correlation and energy resolution distributions at the SAT location.

angle (x') measurements with an accuracy so that the energy resolution is limited by the beam spread. As shown in Fig. 10, there is a good energy-position correlation and a counter size of 0.5 cm provides an energy resolution better than 2%. In addition, the two hodoscopes can provide time measurements with a resolution of few hundred picoseconds. This, together with the long distance from the interaction point, can be used to separate electrons from muons and pions by time of flight measurements.

3.2 The COIL detector

To achieve a higher acceptance we consider now the possibility to tag those $\gamma\gamma$ events corresponding to electrons hitting the SFM coils. With the present design of the machine layout there is some free space at a distance of $\simeq 4.6$ m from the interaction point. The cross section of the beam pipe at this point is shown in Fig. 11: the beams pass through two vacuum chamber sections separated by a free space, 3.5 cm wide, which can host a small tagging detector.

We propose to insert a hodoscope made of scintillating fibers just after a thin window in the compensator vacuum flange. The size of the hodoscope is determined by the profiles of the electrons in this region. With a ± 1.5 cm wide and ± 3.0 cm high detector centered on the machine axis, we estimate a single tagging acceptance of $\simeq 10\%$.

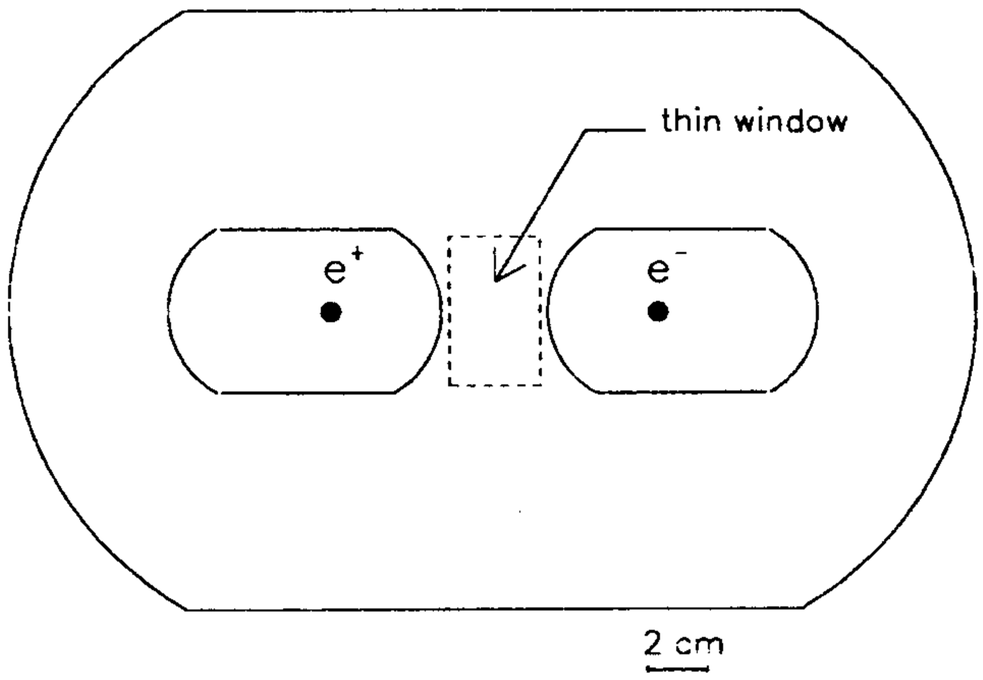

Figure 11: The vacuum flange of the compensator at a distance of 4.6 m from the interaction point. The $\gamma\gamma$ electrons hitting the thin window are detected.

3.3 Background contamination

As the tagged electrons are produced at very small angles, we expect a high background rate from radiative Bhabha ($e^+e^- \to e^+e^-\gamma$), double radiative Bhabha ($e^+e^- \to e^+e^-\gamma\gamma$) and beam-gas bremsstrahlung. Assuming the design single bunch luminosity for DAΦNE of $L_0 = 4.5 \times 10^{30}\ cm^{-2}\ s^{-1}$ we expect a total rate of $\simeq 15\ MHz$ on the SAT and a $\simeq 3\ MHz$ on the COIL detectors for 120 stand bunches. The distribution of this rate over the SAT counters is displayed in Fig. 12. These very high rates ($\simeq 1\ MHz$) together with the necessity of measuring time of flight with high resolution strongly support our suggestion of using scintillating fiber detectors.

Most of the Bhabha events can be vetoed by detecting the γ's with the BREM detector (see Fig. 5). For this purpose a thin window is provided at the SFM exit, extending horizontally over $-10\ cm \leq x \leq -6\ cm$ and vertically over $-1.5\ cm \leq y \leq 1.5\ cm$. We estimate that such a window should tag more than 90% of the γ's.

4 Measurement of the $e^+e^- \to e^+e^-\pi^0\pi^0$ cross section

The only measurement of the $e^+e^- \to e^+e^-\pi^0\pi^0$ process in the mass range which can be studied at DAΦNE has been published by the Crystal Ball collaboration [6].
This measurement was performed with low statistics and without tagging the electrons, which makes background subtraction and errors rather crude. The systematic and statistical errors can be reduced significantly with the new measurements at DAΦNE. To demonstrate this we show in Fig. 13 the number of events expected in one year of data taking $vs.$ the $\gamma\gamma$ mass. If we take these statistical errors for each mass bin and the chiral

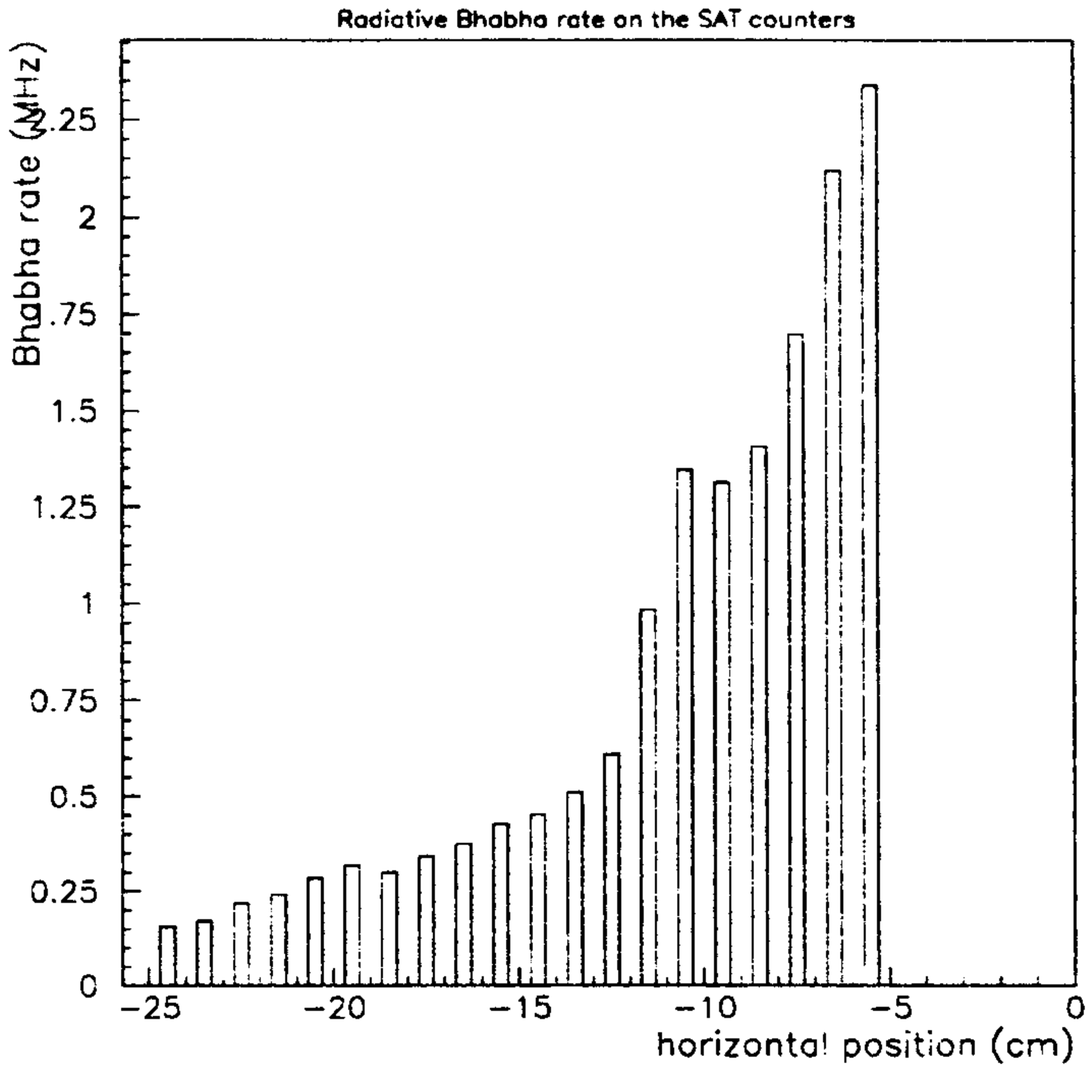

Figure 12: Radiative Bhabha rate on individual fiber bundles of the SAT detector.

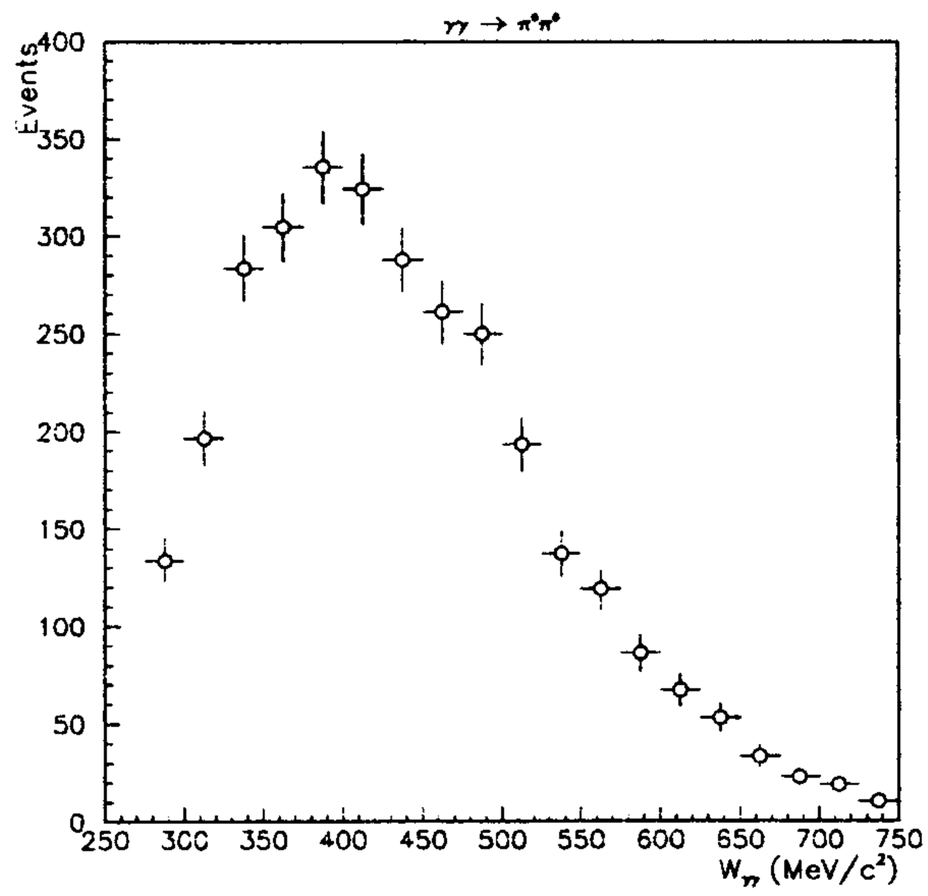

Figure 13: Number of events obtained with both SAT and COIL detectors in one year (10^7 s) of data taking at DAΦNE as a function of the $W_{\gamma\gamma}$ mass. A mass bin of 25 MeV/c^2 is assumed.

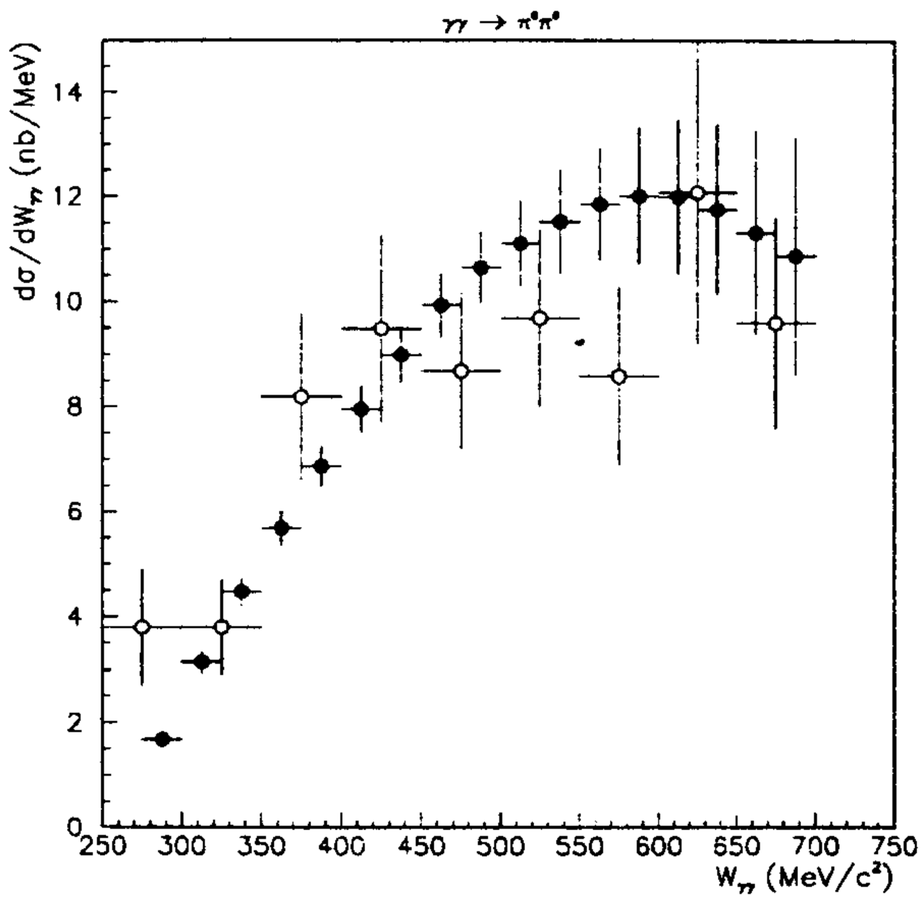

Figure 14: The 2-loop $\gamma\gamma \to \pi^0\pi^0$ cross section [12] measured with both the SAT and COIL detectors, compared to the Crystal Ball data [6] (empty circles). The 1-loop calculations (not shown) give significantly lower cross sections in the near threshold region.

two loop cross section given in ref [12] we can estimate the significance of the proposed measurements. This is done in Fig. 14 where we compare our expected results with the Crystal Ball data [6]. The DAΦNE measurements would be extremely useful to evaluate the importance of the two loop corrections near threshold, where one and two loop cross sections are significantly different. Due to better identification of the final state the systematic errors should be much lower than those of ref [6].

5 Conclusions

We have shown that $\gamma\gamma$ electrons produced at very small angles can be detected with a reasonable acceptance in DAΦNE.
These tagging systems include two COIL detectors to tag particles hitting the SFM coils, and two SAT detectors to tag particles passing through the SFM. To reject radiative Bhabha events we propose to detect the high energy photons in coincidence with the tagged electrons using a BREM detector. The COIL and BREM detectors require thin windows at the last flange of the compensator vacuum chamber and at the SFM exit face. A preliminary design of the SAT and COIL detectors have been presented together with a discussion on the significance of new measurements of the $\gamma\gamma \to \pi^0\pi^0$ cross section at DAΦNE.

References

[1] A. Courau, $\gamma\gamma \to \pi\pi$ **near Threshold at DAΦNE**, Proceedings of the Frascati Workshop for Detectors and Physics at DAΦNE, Frascati, Italy, April 9-12, (1991) 373

[2] Particle Data Group, Phys. Rev. D45 part II (1992) 1.

[3] For a review, see Ch. Berger and W.Wagner, Phys. Rep. 146 (1987) 1, and references therein.

[4] J. Bijnens and F. Cornet, Nucl. Phys. B296 (1988) 557.
J. Bijnens, S. Dawson and G. Valencia, Phys. Rev. D44 (1991) 3555.

[5] J.F. Donoghue, B.R. Holstein and Y.C. Lin, Phys. Rev. D37 (1988) 2423.
J.F. Donoghue and B.R. Holstein, Phys. Rev. D40 (1989) 2378.
P. Ko, Phys. Rev. D41 (1990) 1531.
J. F. Donoghue, C. Ramirez and G. Valencia, Phys. Rev. D39 (1989) 1947.

[6] Crystal Ball Coll. (H. Marsiskie et al.), Phys. Rev. D14 (1990) 3324.

[7] D.Morgan and M.R.Pennington, Physics Letters B 272 (1991), 134.
M.R.Pennington, **Predictions for $\gamma\gamma \to \pi\pi$: What Photons at DAΦNE Will See**, The DAΦNE Physics Handbook, ed. by L.Maiani, G.Pancheri and N.Paver, INFN, Frascati (1992) 379.

[8] G. Alexander et al., **Two Photon-Physics Capabilities of KLOE at DAΦNE**, Il Nuovo Cimento A107 (1994) 837.

[9] G. Pancheri, Phys. Lett. B315 (1993) 477.

[10] V.N. Baier et al., Physics Reports 78 (1981) 293.
M. Greco et al., Phys. Lett. B318 (1993) 635.

[11] M.E. Biagini et al., **Review of *DAΦNE* Lattice**, *DAΦNE* Technical note L-9, (1993).

[12] S. Bellucci, J. Gasser and M. Sainio, Frascati Preprint, LNF-93/077(P), (1993).